Research article

Oxana Semyachkina-Glushkovskaya*, Ivan Fedosov, Alexander Shirokov, Elena Vodovozova, Anna Alekseeva, Alexandr Khorovodov, Inna Blokhina, Andrey Terskov, Aysel Mamedova, Maria Klimova, Alexander Dubrovsky, Vasily Ageev, Ilana Agranovich, Valeria Vinnik, Anna Tsven, Sergey Sokolovski, Edik Rafailov, Thomas Penzel and Jürgen Kurths

Photomodulation of lymphatic delivery of liposomes to the brain bypassing the blood-brain barrier: new perspectives for glioma therapy

https://doi.org/10.1515/nanoph-2021-0212
Received May 3, 2021; accepted June 23, 2021;
published online July 9, 2021

Abstract: The blood-brain barrier (BBB) has a significant contribution to the protection of the central nervous system (CNS). However, it also limits the brain drug delivery and thereby complicates the treatment of CNS diseases. The development of safe methods for an effective delivery of medications and nanocarriers to the brain can be a revolutionary step in the overcoming this limitation. Here, we report the unique properties of the lymphatic system to deliver tracers and liposomes to the brain meninges, brain tissues, and glioma in rats. Using a quantum-dot-based 1267 nm laser (for photosensitizer-free generation of singlet oxygen), we clearly demonstrate photostimulation of lymphatic delivery of liposomes to glioma as well as lymphatic clearance of liposomes from the brain. These pilot findings open promising perspectives for photomodulation of lymphatic delivery of drugs and nanocarriers to the brain pathology bypassing the BBB. The lymphatic "smart" delivery of liposomes with antitumor drugs in the new brain tumor branches might be a breakthrough strategy for the therapy of gliomas.

Keywords: glioma; liposomes; lymphatic backroad to the brain; photostimulation; rats.

1 Introduction

The blood-brain barrier (BBB) is a major obstacle for effective delivery of therapeutic compounds to the brain, imposing size and biochemical restriction on the passage of molecules [1]. Gliomas are the most common tumor of the central nervous system (CNS). However, the presence of the BBB blocks an effective delivery of anticancer drugs into brain tumors and leads to treatment failure. Indeed, malignant gliomas (MG) are highly invasive and use the perivascular space (PVS) for invasion and co-opt existing vessels as a satellite tumor form [2]. In the early stages, glioma develops through normal brain vessels with the intact BBB that limits a pharmacological treatment of the newly formed tumor. A cure for MG will only be possible if the invasive brain tumor branches will be adequately treated [3, 4]. Therefore, there is a growing need to develop safe methods bypassing the BBB and blood-tumor barriers for effective therapy of MG.

The lymphatic system of the brain and the meninges can be a good candidate for brain drug delivery. The classical characteristic of the CNS is a lack of lymphatic vessels (LVs). However, it has become more and more evident that

*Corresponding author: Oxana Semyachkina-Glushkovskaya, Humboldt University, Newtonstrasse 15, 12489 Berlin, Germany; and Saratov State University, Astrakhanskaya 82, 410012 Saratov, Russia, E-mail: glushkovskaya@mail.ru. https://orcid.org/0000-0001-6753-7513
Ivan Fedosov, Alexandr Khorovodov, Inna Blokhina, Andrey Terskov, Aysel Mamedova, Maria Klimova, Alexander Dubrovsky, Vasily Ageev, Ilana Agranovich, Valeria Vinnik and Anna Tsven, Saratov State University, Astrakhanskaya 82, 410012 Saratov, Russia
Alexander Shirokov, Saratov State University, Astrakhanskaya 82, 410012 Saratov, Russia; and Institute of Biochemistry and Physiology of Plants and Microorganisms, Russian Academy of Sciences, Prospekt Entuziastov 13, 410049 Saratov, Russia
Elena Vodovozova and Anna Alekseeva, Shemyakin-Ovchinnikov Institute of Bioorganic Chemistry, Russian Academy of Sciences, Miklukho-Maklaya 16/10, 117997 Moscow, Russia
Sergey Sokolovski and Edik Rafailov, Optoelectronics and Biomedical Photonics Group, AIPT, Aston University, Birmingham, B4 7ET, UK
Thomas Penzel, Saratov State University, Astrakhanskaya 82, 410012 Saratov, Russia; and Charité-Universitätsmedizin Berlin, Sleep Medicine Center, Charitéplatz 1, 10117 Berlin, Germany
Jürgen Kurths, Saratov State University, Astrakhanskaya 82, 410012 Saratov, Russia; and Potsdam Institute for Climate Impact Research, Telegrafenberg A31, 14473 Potsdam, Germany

the CNS is not a passive "immune-privileged" organ, but it is rather a compartment demonstrating highly immune responses [5–7]. Recent studies have identified entry and exit points for immune cells, cytokines, and brain-derived antigens or waste molecules through distinct anatomical routes in the meninges [6–8]. The meningeal "door" might allow for the BBB bypass, providing an interface for peripheral immune system interaction with the CNS, and could play an important role in drug delivery to the MG.

In our previous work, we reported photostimulation (PS) of the meningeal lymphatic vessels (MLVs) [5–11] using a quantum-dot 1267 nm laser, which can directly generate singlet oxygen ($^1O_2$) from the triplet oxygen state without photosensitizers [12, 13]. We uncovered that PS stimulates the clearance of macromolecules from the brain via MLVs as well as PS causes an increase in the permeability of the lymphatic endothelium to macrophages [9, 10]. In our pilot experiments on rats, we demonstrated laser-suppression of glioma growth that was associated with the activation of the lymphatic drainage system, stimulation of apoptosis, decrease of autophagy, and proliferation of glioma cells [11]. These findings open new strategies for therapy of brain diseases, including glioma by modulation of the lymphatic functions via PS.

Liposomes, as nanoscale drug carriers, are a promising drug delivery system [14–21] that can encapsulate both hydrophilic and hydrophobic drugs. Hydrophilic drugs are encapsulated in an aqueous core, and lipophilic drugs are encapsulated in a hydrophobic region of the lipid bilayer. The lipid bilayer of liposomes is composed on the basis of phospholipids and is very similar to cell membranes. In addition, liposomes offer numerous advantages, including targeting capability, long-term efficacy, improved drug stability, lowered drug toxicity, and increased circulation time [15, 18]. Liposomes are also capable of achieving targeting by modifying proteins, antibodies, aptamers, or polypeptides [14]. These properties of liposomes have attracted interest in their development as promising transporters to deliver antitumoral drugs to the CNS and thus, to improve brain drug targeting and therapeutic efficiency [14, 16, 17].

Among different types of liposomes, those incorporated with gangliosides are of greatest interest for brain drug delivery [17, 19]. Gangliosides consist of a hydrophilic sialic acid terminal sugar and a hydrophobic ceramide moiety, they widely exist in neural tissue of vertebrates and have been reported to modulate ion transport, neuronal differentiation, G protein-coupled receptors, immune system reactivity, and neuroprotective signaling [20, 21]. More importantly, liposomes consisted of one of a ganglioside monosialotetrahexosylganglioside (GM_1) can overcome the BBB and treat neurological disease [17, 19]. Recently we demonstrated photodynamic opening of the BBB for the intravenously injected GM_1-liposomes [22].

In this work, we aim to study a lymphatic delivery of GM_1-liposomes to the brain and fluorescent glioma in rats, bypassing the BBB. We also sought to examine the modulation of lymphatic transport of liposomes by PS to and from the rat brain.

2 Results

2.1 Lymphatic backroad to the brain and the meninges

The deep cervical lymph nodes (dcLNs) play a crucial role in the crosstalk between the brain and the peripheral lymphatic system [6, 23–27]. It is assumed that the cervical lymph nodes can be an anatomical platform for brain drug delivery [7, 27]. Here, we test this hypothesis and study a lymphatic delivery of liposomes and Evans Blue dye to the brain meninges and tissues after its injection into dcLN.

To determine the effective time for lymphatic delivery of tracer to the meninges, we analyzed the presence of Evans Blue in the meninges 1, 2, and 3 h after dye injection. Figure 1 a-c demonstrate confocal images of the meninges labeled with the lymphatic marker, such as Lyve-1, and the time-dependent distribution of Evans Blue in the lymphatic network. Quantitative analysis revealed a gradual increase in time of the Evans Blue fluorescent signal in the meninges. The fluorescence of Evans Blue in the meninges reached a maximum of 3 h after the dye injection in dcLN. Indeed, the intensity of the fluorescent signal from Evans Blue in the meninges was 3.90-fold higher ($p < 0.001$) versus 1 h after the dye injection and 1.59-fold higher ($p < 0.001$) versus 2 h after the clearance of Evans Blue from the brain (Figure 1f). These findings allowed us to conclude that 3 h after injection of tracer is enough for its lymphatic delivery to the meninges. Therefore, this time was used in our further experiments.

A number of studies showed a retrograde flow in the PVS in the brain that is also typical for the peripheral lymphatic system [28–30]. To answer the question, how tracers are delivered to the brain from dcLN, we monitored *in vivo* the presence of Evans Blue in the meninges using ligation of the cervical LVs in upper and lower dcLN (Figure 1g). Our finding showed the appearance of dye in the meninges (3 h after its injection into the dcLN) in the case of ligation of the cervical LVs lower but not upper dcLN suggesting a retrograde lymphatic flow of Evans blue from dcLN to the brain.

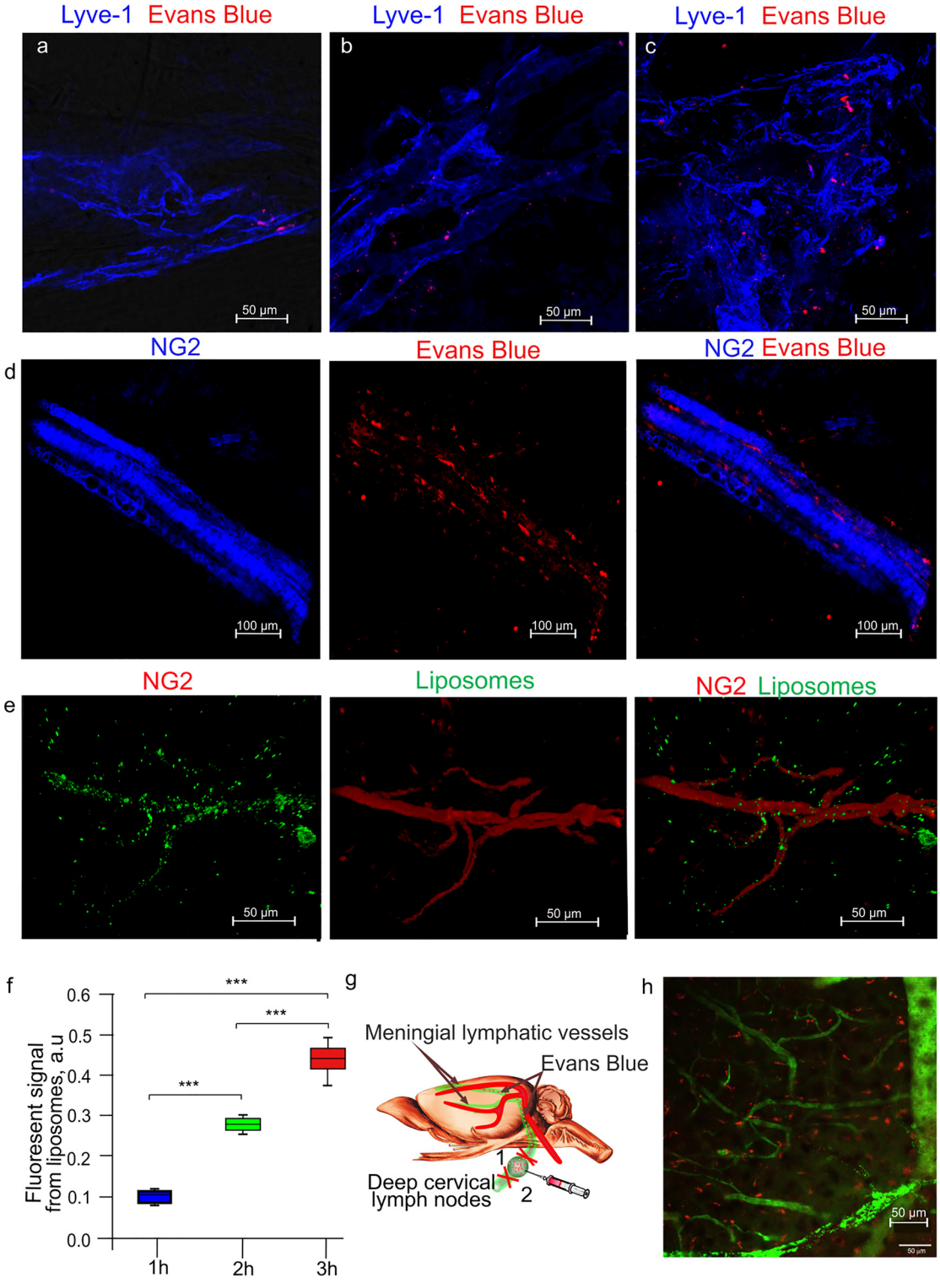

Figure 1: The lymphatic backroad to the brain: **a**–**c** – Representative images of the distribution of Evans Blue in the meninges labeled with Lyve-1 in rats 1 h (a), 2 h (b), and 3 h (c) after the dye injection in dcLN; **d** – Representative images of the presence of Evans Blue along the meningeal blood vessels labeled with marker of pericytes (neuron-glial antigen 2 – NG2) 3 h after its injection in dcLN; **e** – Representative images of the presence of liposomes along the meningeal blood vessels labeling with NG2 3 h after its injection in dcLN; **f** – Quantitative analysis of the signal intensity from Evans Blue in the meninges 1, 2, and 3 h after the dye injection in dcLN, ***$p < 0.001$ between groups at $t = 1$, 2, and 3 h after the dye injection, $n = 7$ in each time point; **g** – Schematic illustration of the cervical LVs for the study of lymphatic pathways of dye delivery from dcLN; **h** – Real-time confocal imaging of the retrograde lymphatic pathway of Evans Blue delivery to the meninges 3 h after dye injection in dcLN and ligation of the cervical LVs below dcLN.

Next, we analyzed a lymphatic delivery of liposomes to the meninges 3 h after its injection into the dcLN. Figure 1e illustrates the perivascular route of lymphatic delivery of liposomes to the meninges. This is like the results we observed using Evans Blue (Figure 1d). These data suggest that both tracers (liposomes and Evans Blue) were delivered to the meninges via MLVs, which are localized along the meningeal veins [6, 24]. To confirm this fact, we studied the lymphatic delivery of liposomes to the meninges using the lymphatic (lymphatic vessel endothelial hyaluronan receptor 1, Lyve-1) and the blood vessel (neuron-glial antigen 2, NG2) markers. Figure 2 clearly demonstrates the presence of liposomes in MLVs but not in the meningeal blood vessels, suggesting a lymphatic pathway of their traveling from dcLN to the meninges.

Previous work has demonstrated that LVs are present directly in the human brain debating that the cerebral LVs can deliver metabolites and molecules from the PVS to the brain tissue [31]. Although LVs have not been found in the rodent brain yet, it is reasonable to expect delivery of liposomes from the PVS directly to the rat brain. To test this hypothesis, we examined brain slices labeled with the astrocytic (glial fibrillary acidic protein, GFAP) and the blood vessels endothelium (NG2) markers obtained from rats with the injection of liposomes into the dcLNs (3 h after injection). Figure 2 demonstrates the distribution of

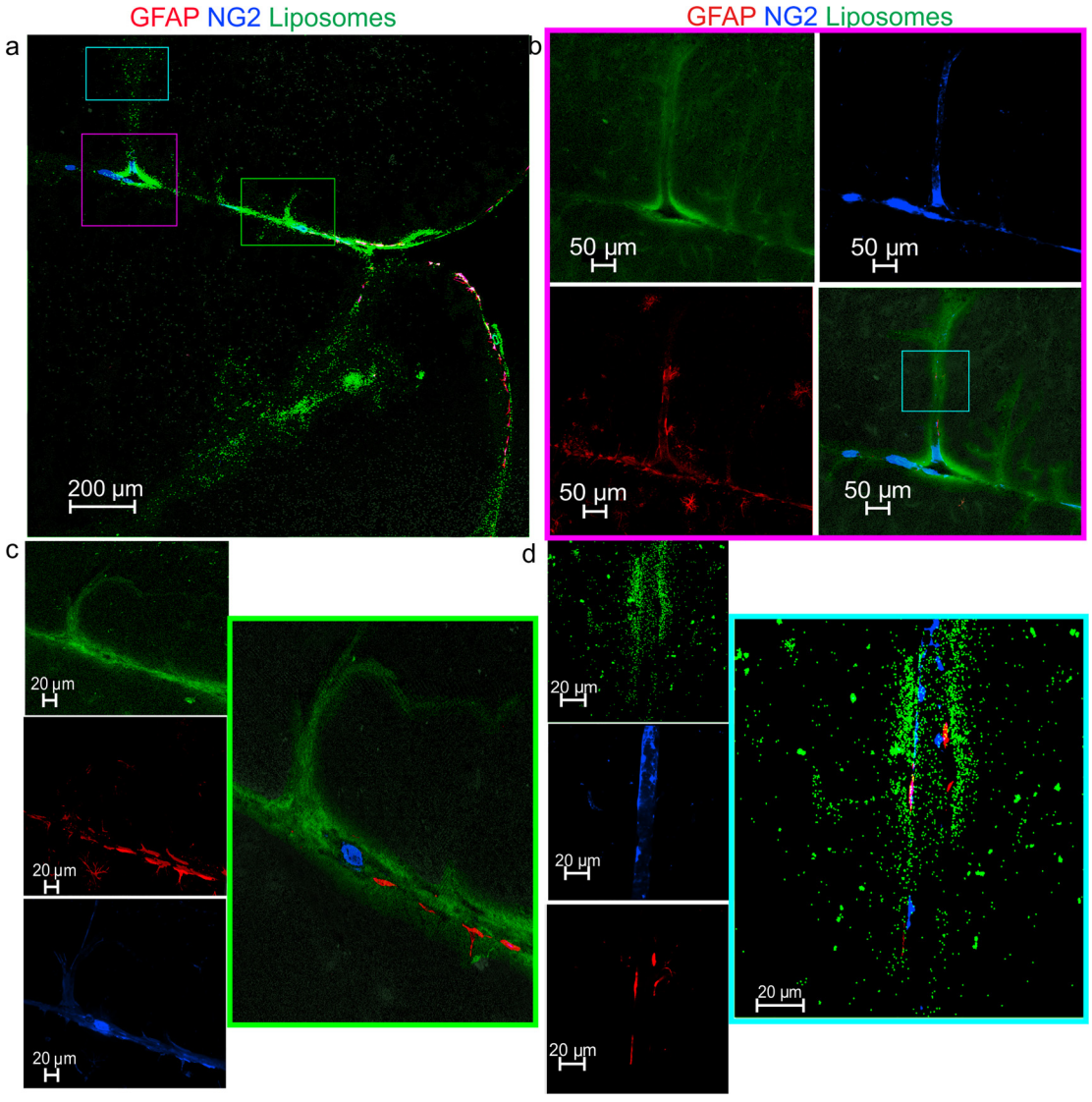

Figure 2: The lymphatic delivery of liposomes to the brain: **a** – Representative images of the brain tissues labeled with GFAP (astrocytic marker) and NG2 (a marker for the pericytes in the blood vessel): **b–d** – Representative images of the three regions of interest demonstrating the distribution of liposomes in the brain parenchyma.

liposomes in the PVS and between the astrocyte endfeet, i.e. in the brain parenchyma.

Thus, these findings evidently demonstrate that dcLNs are an anatomical platform for communication between the brain and the peripheral lymphatic system. The Evans Blue and liposomes can be delivered from the dcLN to the brain meninges and parenchyma via the lymphatic backroad.

2.2 Photomodulation of lymphatic delivery of liposomes to glioma

In this step, we anticipated answering two questions (i) whether liposomes deliver to glioma via the lymphatic pathway and (ii) how does PS modulate this process? The liposomes were injected into the dcLN of rats with fluorescent glioma and allowed to circulate in the lymphatic system for 3 h in both animal groups treated and untreated by PS (Figure 3d). Additionally, Evans Blue dye was injected into the tail vein to study the BBB permeability in these groups. Figure 3a and b illustrate the confocal imaging of fluorescent glioma with the spreading of liposomes in tumor tissues and the leakage of Evans Blue, suggesting the BBB disruption.

Our findings uncovered that the distribution of liposomes among glioma cells was higher in the PS treated group versus the untreated animals. Indeed, Figure 3c shows that the intensity of the fluorescent signal from liposomes in the brain was 1.5-fold higher (0.53 ± 0.02 a.u. vs. 0.35 ± 0.05 a.u., $p < 0.001$, $n = 7$) in the group PS-treated versus the untreated animals.

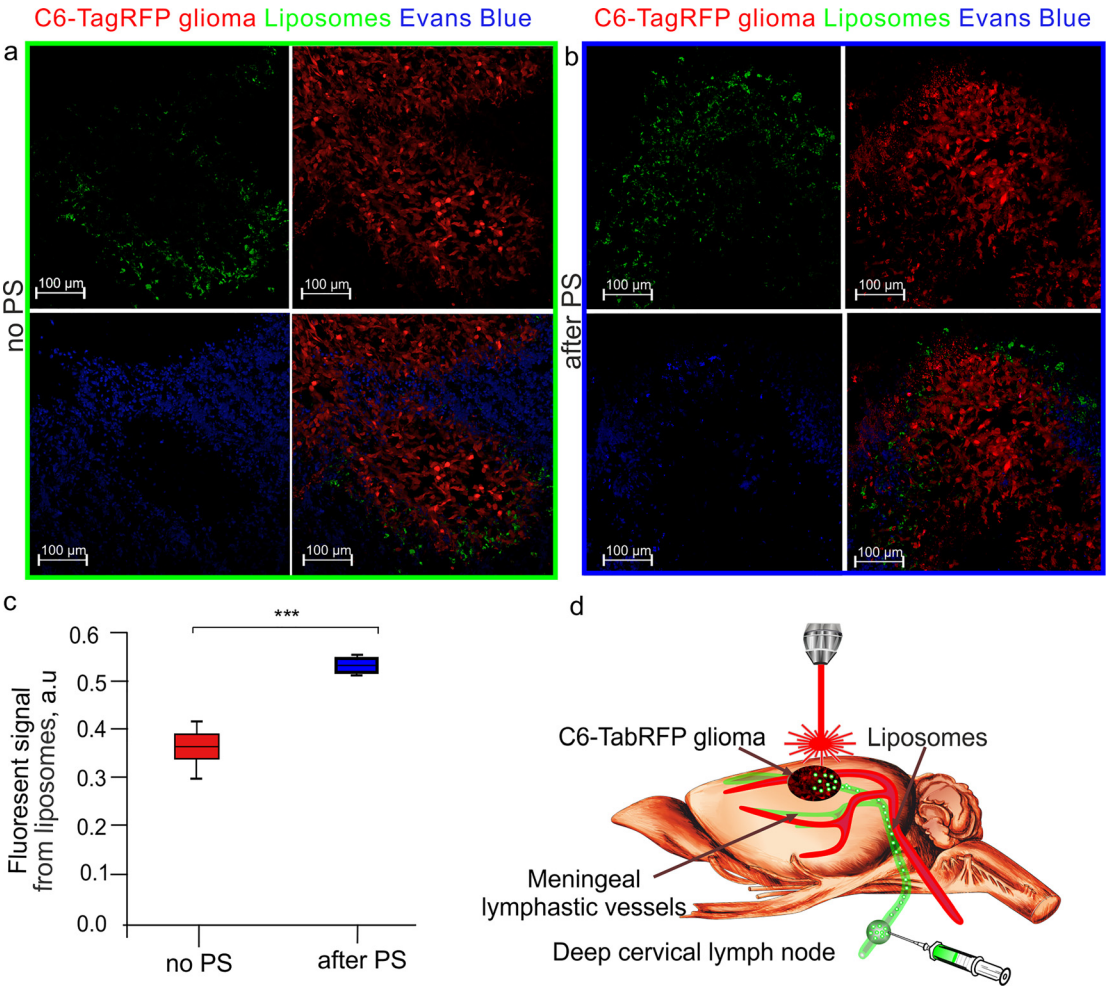

Figure 3: The photostimulation (PS) of lymphatic delivery of liposomes to glioma: **a** and **b** – Representative images of liposomes and the Evans Blue fluorescence in the glioma tissues in the untreated group (a) and the group treated by PS (b); **c** – Quantification of the intensity of the fluorescent signal from liposomes in the brain of treated and untreated rats by PS, ***$p < 0.001$ between groups, $n = 7$ in each group; **d** – Schematic illustration of the experimental design.

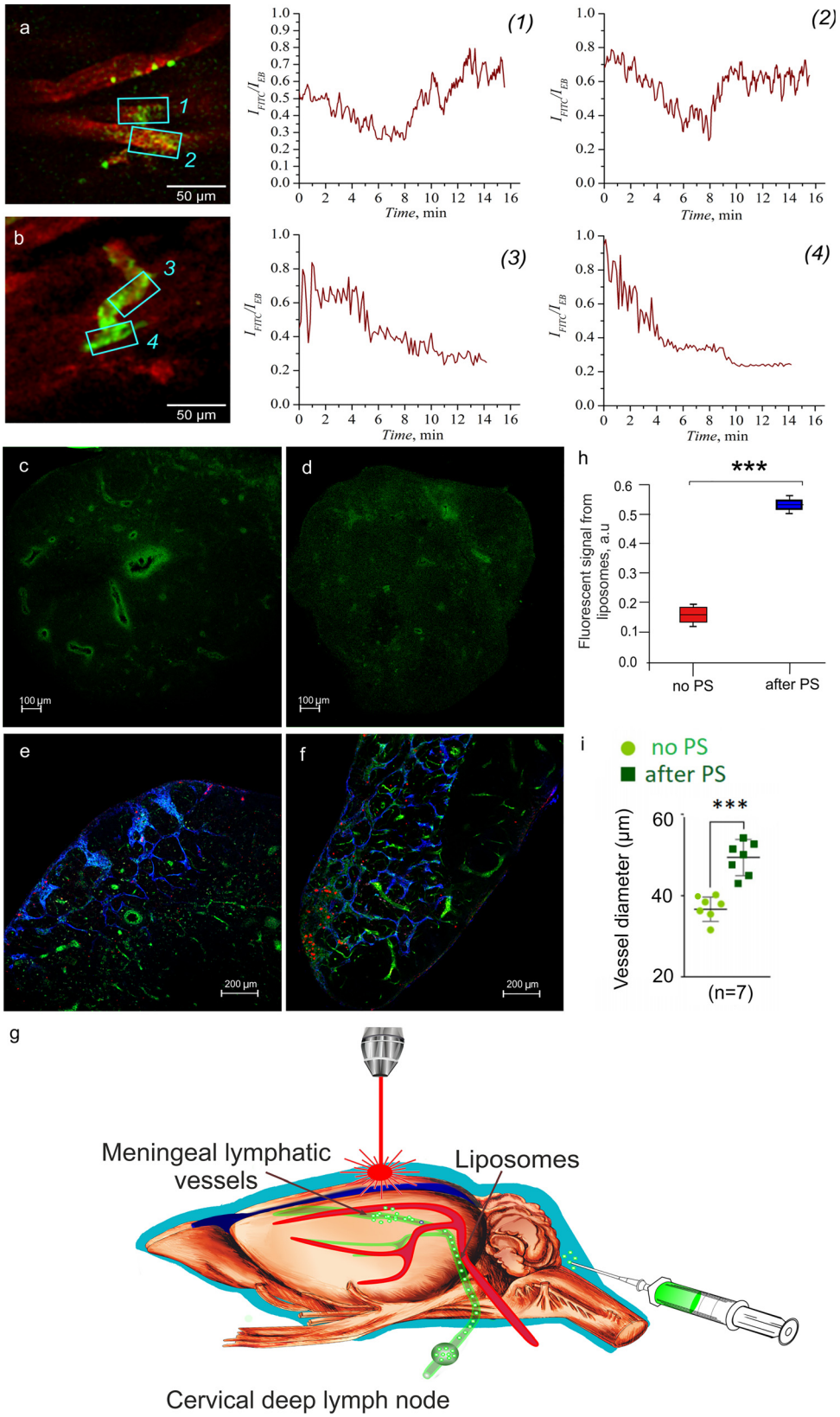

Figure 4: The photostimulation of lymphatic clearance of liposomes from the brain: **a** and **b** – Real-time confocal images and kinetics of the fluorescent signal intensity (1–4) from liposomes in the cervical LVs after their injection into the cisterna magna in the PS-treated (a) and the untreated (b) groups. Blue rectangles denote regions of interest (ROIs) used to measure the averaged intensity of fluorescence (1–4); an

The permeability of the BBB to Evans Blue was analyzed using the spectrofluorometric assay. The results revealed that the leakage of Evans Blue was much lesser in the PS-treated versus the untreated groups (3.73 ± 0.82 μg/g tissue vs. 7.81 ± 1.20 μg/g tissue, $p < 0.001$, $n = 7$ in each group). Nevertheless, both groups demonstrated the BBB permeability to Evans Blue (3.73 ± 0.82 μg/g tissue vs. 0.11 ± 0.09 μg/g tissue, $p < 0.001$ for the PS-treated group and 7.81 ± 1.20 μg/tissue vs. 0.11 ± 0.09 μg/g tissue, $p < 0.001$ for the untreated group, $p < 0.001$, $n = 7$ in each groups). Thus, the treated by PS group demonstrated the more preserved BBB versus the untreated group. This observation can be explained by the fact that PS might in parallel stimulate lymphatic clearing of the molecules from the brain [32]. To confirm this fact, in the final steps we studied whether PS affects the lymphatic clearance of liposomes from the brain.

2.3 PS-mediated lymphatic clearance of liposomes from the brain

In this step, liposomes were injected into the cisterna magna with further real-time confocal monitoring of their clearance from the subarachnoid space via the separated cervical LVs in the PS-treated and untreated rats (Figure 4g). Our results showed that liposomes green fluorescence was detected within the cervical LVs immediately after their intra-cisterna administration and then the intensity of the fluorescence gradually decreased with respect to the intensity of Evans Blue fluorescence. However, when the 1267 nm laser was turned on, an increase of fluorescence from liposomes was observed. Figure 4C shows an arbitrary ratio of boron-dipyrromethene (BODIPY) fluorescence against Evans Blue fluorescence starting from the moment when the laser was turned on (Figures 1, 2, and 4) and for the same time period for the untreated group (Figures 3 and 4) for which the laser was not applied. Blue rectangles denote regions of interest (ROIs) chosen to measure the averaged fluorescence intensity.

The data obtained *in vivo* experiments were confirmed in *ex vivo* confocal imaging of dcLN obtained from the same rats, in which the cervical LV were monitored in real-time. Figure 4c, d, and h clearly demonstrate the significant spreading of liposomes in LVs of dcLN that was 3.6-fold higher in the PS-treated group versus the untreated group (0.55 ± 0.02 vs. 0.15 ± 0.03, $p < 0.001$, $n = 7$). The PS effects were accompanied by dilation of LVs labeled with Live1/Prox1. Indeed, the average diameter of LVs was 2.7-fold bigger in rats after PS than in untreated animals (52.3 ± 2.3 vs. 31.0 ± 1.3 μm, $p < 0.001$, $n = 7$).

Thus, these results demonstrate that PS activates the clearance of liposomes from the subarachnoid space of the brain via lymphatic pathways.

3 Discussion

To address the overcoming difficulties of effective delivery of medications and nanocarriers to the brain, we tested our hypothesis that the lymphatic system of the brain and the meninges can be a good candidate for brain drug delivery with a focus on glioma. Furthermore, we studied PS effects on the lymphatic transport of molecules as a promising tool for the modulation of lymphatic drug delivery to the brain. Our results clearly demonstrate that dcLNs are an anatomical structure for a unique communication between the brain and the peripheral lymphatic network. Indeed, injection of liposomes and tested tracers in dcLN was accompanied by their delivery to the meninges, brain parenchyma, and glioma. Our findings are consistent with other experimental evidence suggesting that dcLNs are a unique passage, which connects the brain fluid system and the peripheral lymphatics [6, 9, 10, 23–26]. So, dcLNs play a crucial role in the crosstalk between the brain and the peripheral immune system [6, 23, 24]. The injection of blood in the different brain regions causes a humoral immune response in mice generated mainly by dcLNs [25]. Similarly, the injection of serum albumin in the subarachnoid space induces an antibody production by cervical lymph nodes in cats [25, 26]. Serum antibody is reduced after the obligation of the cervical LNs [26]. The dcLNs play an important role in the exchanges of immune cells between the microenvironment of brain tumors and the peripheral immune system [33].

We revealed that molecules (Evans Blue and liposomes) traveled from dcLN to the brain meninges and

arbitrary ratio of BODIPY fluorescence versus fluorescence of Evans Blue since the moment the laser was turned on (1, 2) and for the same time period for the untreated group (3, 4) for which the laser was not applied. Representative of $n = 7$ rats of each group. **c** and **d** – Representative images of the presence of liposomes in dcLNs obtained from the PS-treated (c) and the untreated (d) groups; **e** and **f** – Representative images of LVs in dcLNs obtained from the PS-treated (e) and the untreated (f) groups. Representative of $n = 7$ rats of each group; **h** – Quantification of the intensity of the fluorescent signal from liposomes in dcLNs in the PS-treated and the untreated groups, ***$p < 0.001$ between groups, $n = 7$ in each group; **i** – Diameter of the cervical LVs in dcLNs in the PS-treated and untreated groups; ***$p < 0.001$ between groups, $n = 7$ in each group; **g** – Schematic illustration of experimental design.

parenchyma via the lymphatic backroad. The retrograde movement of tracers into the brain parenchyma was also discussed in other works as physiological properties of the lymphatic/glymphatic mechanisms of exchanges of molecules between the PVS and the brain parenchyma [28–30]. Zhao et al. [22] argued that the injection of fluorescent nanoparticles subcutaneously close to the dcLNs is accompanied by nanoparticles brain delivery through MLVs. It has shown that the injection of choroid plexus cells into the ST36 acupuncture point (Stomach 36 or Zusanli) close to the popliteal LVs causes a neuroprotective effect in mice with Parkinson's disease due to the delivery of injected cells to the brain [34].

In our research, we demonstrate that PS enhances the lymphatic transport of liposomes to glioma and the clearance of these nanocarriers from the subarachnoid space. The infra-red light of 800–1100 nm is widely used for the PS therapy of various brain diseases [35]. However, the infra-red PS has a significant drawback in its limited penetration into the brain due to the high scattering and heating effect [36]. The light wavelength of 1300 nm has less scattering and can penetrate deeper into the brain [37]. In our recent work, we revealed that the glioblastoma growth can be suppressed by a photosensitizer-free laser treatment using a quantum-dot-based 1267 nm laser diode [11]. This wavelength, highly absorbed by oxygen, is capable of turning triplet oxygen into reactive singlet form. Applying a 372 J/cm^2 dose of 1267 nm suppressed glioblastoma growth and increased the survival rate from 34 up to 64% presumably via the PS-activated apoptosis, inhibition of the autophagy, proliferation of the tumor cells, PS of the lymphatic drainage, and clearing functions. Using the same PS dose and design of experiments, here we clearly show that PS increases the lymphatic transport of liposomes to glioma. We assume that the PS effects on the tone of LVs facilitate lymphatic transport of liposomes to glioma. Indeed, these effects were accompanied by dilation of the cervical LVs. In our recent work, we uncover that PS dilates MLVs that are associated with PS-mediated stimulation of lymphatic transport of red blood cells from the brain [38]. These results demonstrate that PS activates the nitric oxide (NO) synthesis in lymphatic endothelium isolated cells and the LVs contractility might be the possible mechanisms responsible for PS of lymphatic clearance of macromolecules from the brain. The PS-mediated dilation of LV can be due to an increase in the activity of endothelial NO synthase [39]. NO is a vasodilator that acts via stimulation of soluble guanylate cyclase to form cyclic-guanosine monophosphate, which activates protein kinase G causing the opening of calcium-activated potassium channels and reuptake of Ca^{2+} from the cytosol. The decrease in the concentration of Ca^{2+} prevents myosin light-chain kinase from phosphorylating the myosin molecule, leading to the relaxation of LVs [40]. The PS-mediated relaxation of LV is closely associated with an increase in the permeability of the lymphatic endothelium via a decrease in the expression of tight junction proteins [9, 10]. The increased lymphatic permeability is a driving force for drainage and clearing functions of LVs. These facts explain our data, which demonstrate that PS activates the clearance of liposomes from the subarachnoid space by modulating the tone of the cervical LVs. This also partly explains why the PS-treated group showed lower levels of Evans Blue in the brain comparing with the untreated group.

In summary, our results demonstrate the unique properties of the lymphatic system to delivery of tracers and liposomes to the brain meninges, brain tissues, and glioma tissues in rats. Using a quantum-dot-based 1267 nm laser (photosensitizer-free generation of singlet oxygen), we clearly show the PS of lymphatic delivery of liposomes to glioma as well as lymphatic clearance of liposomes from the brain. These pilot findings open promising perspectives for photomodulation of a lymphatic delivery of drugs and nanocarriers to the brain with pathologies bypassing the BBB and potentially enabling a breakthrough strategy in therapy of glioma.

4 Methods

4.1 Subjects

Pathogen-free male Wistar rats (200–250 g, two months old) were used in all experiments and were obtained from the National Laboratory Animal Resource Center (Pushchino, Moscow, Russia). The animals were housed under standard laboratory conditions, with access to food and water, *ad libitum*. All procedures were performed in accordance with the "Guide for the Care and Use of Laboratory Animals". The experimental protocols were approved by the Bioethics Commission of the Saratov State University (Protocol No. 7). The experiments were performed in the following groups: (1) and (2) – The Evans Blue (1) and liposomes (2) injection in dcLN for *ex vivo* confocal analysis of tracers presence in the meninges, in the PVS of MLVs, and in the brain, respectively; (3) and (4) – The liposomes injection in dcLN and ligation of the cervical LVs above (3) and below (4) dcLN for *in vivo* confocal images of liposomes in the meninges, respectively; (5) and (6) – The liposomes injection in dcLN for *ex vivo* confocal analysis of the brain in rats with fluorescent glioma without PS (5) and after PS (6), respectively; (7) The liposomes injection in the cisterna magna for *in vivo* and *ex vivo* confocal imaging of the cervical LVs in the same rats; $n = 7$ in each group.

4.2 Synthesis of GM_1-liposomes

Fluorescently-labeled GM_1-liposomes were prepared as described earlier [22]. Briefly, a lipid film obtained from egg yolk phosphatidylcholine (Lipoid GmbH, Germany) – ganglioside GM_1 from bovine brain (Sigma Chemical Co., St. Louis, MO, USA), 9:1 (by mol), and 1 mol% of BODIPY-phosphatidylcholine (λ_{ex} = 497 nm, λ_{em} = 505 nm [41, 42]) was hydrated in physiological saline (phosphate buffer with 1 mM EDTA, pH 7.3; total lipid concentration 25 mM) (Figure 5). The resulting suspension was subjected to seven cycles of freezing/thawing (liquid nitrogen/+40 °C) and extruded 10 times through polycarbonate membrane filters (Nucleopore, USA) with a 100 nm pore diameter using Avanti Mini-extruder (Northern Lipids, Canada). Particle size was measured by dynamic light scattering with the Brookhaven equipment (Brookhaven Instruments Corp. 90Plus Particle Sizing Software ver. 4.02, NY, USA) in at least three runs per sample: effective diameter and polydispersity indexes were 90.2 ± 1.8 nm and 0.071, respectively. The Zeta potential of liposomes of this composition measured using ZetaPALS analyzer (Brookhaven Instruments Corp., Holtsville, NY) [22], was − 48.3 ± 0.9 mV (according to calculations using Smoluchowski approximation).

4.3 Implantation of C6-TagRFP glioma [43]

The rats were pre-treated by premedication with Seduxen (Gedeon Richter, Hungary) in a dose of 50 μg/mL. Afterward, rats were deeply anesthetized with intraperitoneal Zoletil (Virbac, France) in a dose of 100 μg/kg and moved into a stereotaxic head holder and immobilized on the stereotactic system (Narishige, Japan) by fixation of the head. The scalp of the anesthetized rat was shaved and scrubbed with betadine three times followed by an alcohol rinse. Hair was removed at the site of the planned operation and the scalp was cut in this area. An incision was made over the sagittal crest from the bregma to the lambdoidal suture and the periosteal membrane was removed. A small dental drill was used to create a burr hole through the bone without tearing the dura matter in the exposed cranium 0.5 mm anterior and 3 mm lateral to the bregma.

The cell line C6 of rat glioma was obtained from the Russian Cell Culture Collection of Vertebrates, Institute of Cytology, Russian Academy of Sciences (St. Petersburg, Russia). A transfected C6-TagRFP cell line was used for the study of the growth of fluorescent glioblastoma [43]. C6 cells were cultured in Dulbecco's modified eagle medium (DMEM, PanEco, Russia) containing 2.5% fetal calf serum (Biosera), 4 mM glutamine (PanEco, Russia), penicillin (50 IU/mL) and streptomycin (50 mg/mL) (PanEco, Russia). Versen's solution (PanEco, Russia) with the addition of 0.25% trypsin (Gibco) was used to remove cells from the surface of the culture plastic. Cells were cultured in a humid environment in a CO_2 incubator at a temperature of 37 °C, with a content of 5% CO_2. The number of cells was counted on the TC20 Bio-Rad automated cell counter, and the viability analysis was determined using a trypan blue dye. Rat C6 glioma cells were transfected with pTagRFP-C DNA plasmid using the method of liposomal transfection followed by selection using geneticin (G418 antibiotic, neomycin analog) on the base research center "Symbiosis" Institute of Bioorganic Chemistry, Russian Academy of Sciences (Saratov, Russia). The resulting cell line C6-TagRFP has stable cultural and morphological characteristics.

The glioma cells (5 × 105 cells per rat) were injected at a depth of 4.5 mm from the brain surface into the caudate-putamen area with a Hamilton microsyringe in a volume of 15 μL at a rate of 3 μL/min. The duration of implantation did not exceed 10–15 min. The physiological saline (15 μL, Sigma-Aldrich, US) was injected into the same region of

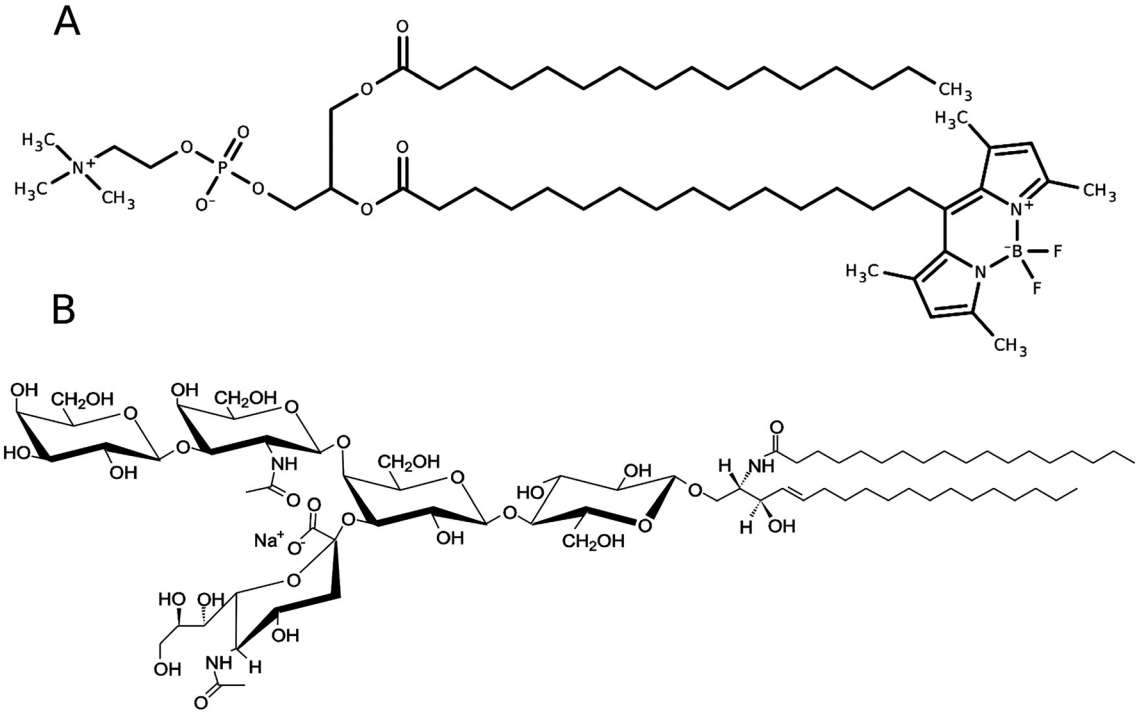

Figure 5: Molecular structures of lipid bilayer components of fluorescently labeled GM_1-liposomes based on egg phosphatidylcholine: A – BODIPY-phosphatidylcholine {1-palmitoyl-2-[15-(4,4-difluoro-1,3,5,7-tetramethyl-4-bora-3*a*,4*a*-diaza-*s*-indacene-8-yl)pentadecanoyl]-*sn*-glycero-3-phosphocholine}; B – shown is a representative structure of ganglioside GM_1 from bovine brain.

the brain in the sham groups. Thereafter, the burr hole was sealed with sterile bone wax and tissue glue and the wound sutured closed with 3–0 absorbable suture material. After the implantation of glioma cells, the wound was closed and treated with a 2%-brilliant green solution. The rats were removed from the stereotaxic head holder, given 0.01 mg/kg buprenorphine, s.c., and 50K bicillin, i.m. and returned to their cages after recovery in the temperature-controlled recovery cage and moved back to the animal facility after recovery. The animal was placed in a clean cage. The growth of fluorescent glioblastoma C6-TurboFP635 in rats was assessed by confocal microscopy using the Leica SP5 confocal laser scanning microscope (Leica, Germany) via optical window using adapted protocol for two-photon imaging of neural activity in awake behavior rodents [44].

4.4 Immunohistochemistry (IHC) and confocal imaging

For confocal imaging of MLVs, we used the protocol for the IHC analysis with the markers for lymphatic vessel endothelial hyaluronan receptor 1 (LYVE1), for the pericytes in the blood vessels, such as the neuron-glial antigen 2 (NG2), and for astrocytes by glial fibrillary acidic protein (GFAP). For the IHC analysis, brain and dcLN tissue were collected and free-floating sections were prepared. The tissue of the brain and dcLN were fixed for 48 h in a 4% saline solution-buffered formalin, then sections of the brain and dcLN with a thickness of 40–50 μm were cut on a vibratome (Leica, Germany). The tissues of dcLN were previously poured into 2% agarose on the saline solution. Sections were processed according to the standard immunohistochemical protocol with the corresponding primary and secondary antibodies. The sections of the mouse brain, meninges, and dcLN were imaged using a Leica SP8 confocal laser scanning microscope (Leica, Germany). The antigen expression was evaluated on free-floating sections according to the standard method of simultaneously combined staining of the drug (Abcam protocols for free-floating sections). The nonspecific activity was blocked by a 2-h incubation at room temperature with 10% BSA in a solution of 0.2% Triton X-100 in phosphate-buffered saline (PBS). Solubilization of cell membranes was carried out during 1-h incubation at room temperature in a solution of 1% Triton X-100 in PBS. Incubation with primary antibodies in a 1:500 dilution took place overnight at 4 °C: with rat antibodies to Lyve-1 (1:500; NBP1-43411AF488; Novus Biologicals, Centennial, Colorado, USA); mouse antibodies to NG2 (1:500; ab50009; Abcam, Biomedical Campus Cambridge, Cambridge, UK) and rabbit antibodies to GFAP (1:500; ab207165; Abcam, Biomedical Campus Cambridge, Cambridge, UK). At all stages, the samples were washed 3–4 times with 5-min incubation in a washing solution. After that, the corresponding secondary antibodies were applied (goat anti-rat IgG (H + L) Alexa Four 405; goat anti-mouse IgG (H + L) Alexa Four 555, and goat anti-rabbit IgG (H + L) Alexa Four 647; Invitrogen, Molecular Samples, Eugene, Oregon, USA). At the final stage, the sections were transferred to the glass and 15 μL of mounting liquid (50% glycerin in PBS with the diamidino-2-phenylindole (DAPI) at a concentration of 2 μg/mL) was applied to the section, then the preparation was covered with a cover glass and confocal microscopy was performed.

For IHC with BODIPY-liposomes, the brains were fixed with 4% neutral buffered formalin. After fixation, the brains were cryoprotected using 20% sucrose in PBS (10 mL/brain mouse) for 48 h at 4 °C. The brains were frozen in hexane cooled to −32 to −36 °C. Crysection (14 μm) of parietal cortex were collected on poly-L-Lys, Polysine Slides (Menzel-Glaser, Germany) using cryotome (Thermo Scientific Microm HM 525, Germany) and a liquid for fixing a Tissue-Tek sample (Sakura Finetek, USA). Cryosections were blocked in 150 μL 10% BSA/PBS for 1 h, then incubated overnight at 4 °C with 130 μL anti-rat antibodies to Lyve-1 (1:500; NBP1-43411AF488; Novus Biologicals, Centennial, Colorado, USA); mouse antibodies to NG2 (1:500; ab50009; Abcam, Biomedical Campus Cambridge, Cambridge, UK) and rabbit antibodies to GFAP (1:500; ab207165; Abcam, Biomedical Campus Cambridge, Cambridge, UK). After several rinses in PBS, slides were incubated for 1 h with 130 μL fluorescent-labeled secondary antibodies on 1% BSA/PBS goat anti-rat IgG (H + L) Alexa Four 405; goat anti-mouse IgG (H + L) Alexa Four 555, and goat anti-rabbit IgG (H + L) Alexa Four 647; Invitrogen, Molecular Samples, Eugene, Oregon, USA). At the final stage, the sections were transferred to the glass and 15 μL of mounting liquid (50% glycerin in PBS with DAPI at a concentration of 2 μg/mL) was applied to the section, then the preparation was covered with a cover glass and confocal microscopy was performed.

4.5 Quantitative analysis of confocal images

The analysis of fluorescence of BODIPY-liposomes in the testes tissues was carried out on a microscopic system with automatic analysis of the obtained photos of Ariol SL50 (Genetix, UK). The software module PathVysion (Music, Inc. Applied Imaging) determined the total area of the histological preparation and calculation the fluorescence intensity in the whole brain or dcLN slices. In all cases, 10 ROIs were analyzed.

For the quantitative analysis of intensity signal from Evans Blue in the meninges, ImageJ was used for image data processing and analysis. The areas of specific signals from dye were calculated using the plugin “Analyze Particles” in the “Analyze” tab, which calculates the total area of Evans Blue fluorescence intensity tissue elements – the indicator “Total Area”. In all cases, 10 ROIs were analyzed.

The diameters of the cervical LVs were measured by tracing the width of vessels along the direction of the vessel running from the cortical to medulla sinuses every 20-μm interval in the entire lymphatic network of whole-mount dcLN samples as ROI using ImageJ software (NIH).

4.6 Real-time images of the cervical lymphatic vessels and the meninges

Images of the cervical LVs and Evans Blue in the meninges were acquired *in vivo* using Nikon A1R confocal microscope with a 10 × 0.45 dry lens (Nikon Corp., Japan). Images were acquired continuously with 3 s intervals since the fluorescent liposomes or Evans Blue was administered in dcLN. The intensity of fluorescence was measured in arbitrary units with homemade software developed using LabVIEW and NI Vision toolkit (National Instruments Corp., USA). The intensity of fluorescence was measured with software developed using LabVIEW and NI Vision (National instruments Corp., USA). Series of two-channel images captured with a confocal microscope was converted into tiff format with Fiji [45]. To minimize the effect of animal movement pattern recognition-based coordinate system correction was performed. It allows to link rectangular ROI to the vessels pattern and to ensure correct intensity measurements. The intensity of fluorescence was measured in both channels (BODIPY and Evans Blue) over rectangular ROI of 20–40 μm in size rotated to fit the vessel as it is

shown in Figure 4c. The resulting intensity was then calculated as an averaged value over approximately 1500 pixels constituting ROI. To correct some minor intensity fluctuations caused by vessel displacement in the axial direction the ratio of BODIPY to Evans Blue intensity was calculated. The ratio represents variations of liposome intensity fluctuations induced with both liposome movement and bleaching with respect to the fluorescence of Evans Blue that is not subjected to photobleaching and that was administered beforehand to ensure stable staining of LVs.

4.7 Spectrofluorometric assay of Evans Blue extravasation

Evans Blue dye (Sigma Chemical Co., St. Louis, Missouri, 2 mg/25 g mouse, 1% solution in physiological 0.9% saline) was injected into the femoral vein and circulated in the blood for 30 min. Then, the rats were decapitated, and their brains were quickly collected. At the end of the circulation time, mice were decapitated, their brains and blood were quickly collected and placed on ice (no anticoagulation was used during blood collection). Prior to brain removal, the brain was perfused with saline to wash out the remaining dye in the cerebral vessels. The level of Evans Blue in the brain was evaluated in accordance with the recommended protocol [46].

4.8 Laser radiation scheme and dose calculation

A fiber Bragg grating wavelength locked high-power laser diode (LD-1267-FBG-350, Innolume, Dortmund, Germany) emitting at 1267 nm was used as a source of irradiation. The laser diode was pigtailed with a single-mode distal fiber ended by the collimation optics to provide a 5 mm beam diameter at the specimen. The rats were recovered after the glioma cells transplantation for seven days. Thereafter, the head of rats was shaved and the scalp was removed, then they were fixed in a stereotaxic frame and irradiated in the area of the glioma cells injection with a near-infrared laser using the algorithm: 17 min PS + 5 min pause + 17 min PS + 5 min pause + 17 min PS of 100 mW laser power intensity with the total dose applied of 1611 J/cm^2 (on the surface of skull) and 470 J/cm^2 (on the surface of the brain, taking in account skull absorption of 65% and scattering initial laser irradiation from 5 to 6 mm [11]) under inhalation anesthesia (1% isoflurane at 1 L/min N_2O/O_2 – 70/30 ratio) [11]. The laser doses were calculated as follows:

$$D = 0.35 * \frac{P * T}{1.2 * S} \quad (1)$$

where D is irradiation dose; 0.35 and 1.2 are scull absorbance and scattering coefficients, correspondently; S is square of the laser beam on the brain cortex (cm^2); P is a laser irradiation power on the scull surface (W); and T is the full laser irradiation time (s).

4.9 Statistical analysis

The results are presented as mean ± standard error of the mean. Differences from the initial level in the same group were evaluated by the Wilcoxon test. Intergroup differences were evaluated using the Mann–Whitney test and the two-way analysis of variance (ANOVA-2) and post hoc analysis with Duncan's rank test. The significance levels were set at $p < 0.05$–0.001 for all analyses.

Acknowledgments: The authors thank Saranceva Elena for the preparation of the figures and the research center "Symbiosis" IBPPM RAS for their support with confocal microscopy and preparation of glioma cultures within research project no. GR 121031100266-3.

Author contributions: O.S.-G., J.K., and E.R initiated and supervised this work. A.Sh and A.T. performed *ex vivo* confocal analysis; I.F., A.D., and V.A. performed *in vivo* confocal analysis; E.V. and A.A. made a synthesis of liposomes; and A.K, I.B., A.M., M.K., I.A., V.V., and A.T. performed most of the experiments. E.S. prepared the figures. O.S.-G., J.K., S.S, and E.R reviewed all results and wrote the manuscript. J.K. and T.P. participated in the discussions of the results and commented on the manuscript. All authors were also involved in the results discussion and manuscript reviewing and editing.

Research funding: S.-G.O., I.V., A.K., I.B., A.T., A.M., M.K., A.D., V.A., I.A., V.V., A.T., T.P., and J.K. were supported by RF Governmental Grant № 075-15-2019-1885, Grant from RSF № 20-15-00090 and 19-15-00201, Grant from RFBR 19-515-55016 China a, 20-015-00308-a. E.R. and S.S. gratefully acknowledge funding from EU's H2020 FET OPEN NEUROPA project under Grant Agreement No. 863214.

Conflict of interest statement: The authors declare no conflicts of interest regarding this article.

References

[1] W.W. Pardridge, "CSF, blood-brain barrier, and brain drug delivery," *Expert Opin. Drug. Deliv.*, vol. 13, no. 7, pp. 963–975, 2016.

[2] S. Watkins, S. Robel, I. F. Kimbrough, S. M. Robert, G. Ellis-Davies, and H. Sontheimer, "Disruption of astrocyte–vascular coupling and the blood–brain barrier by invading glioma cells," *Nat Commun*, vol. 5, p. 4196, 2014.

[3] D. Wang, C. Wang, L. Wang, and Y. Chen, "Comprehensive review in improving delivery of small-molecule chemotherapeutic agents overcoming the blood–brain/brain tumor barriers for glioblastoma treatment," *Drug Deliv.*, vol. 26, no. 1, pp. 551–565, 2019.

[4] J.N. Sarkaria, L. S. Hu, I. F. Parney, et al., "Is the blood-brain barrier really disrupted in all glioblastomas? A critical assessment of existing clinical data," *Neuro Oncol.*, vol. 20, no. 2, pp. 184–191, 2018.

[5] R. O. Weller, I. Galea, R. O. Carare, and A. Minagar, "Pathophysiology of the lymphatic drainage of the central nervous system: Implications for pathogenesis and therapy of multiple sclerosis," *Pathophysiology*, vol. 17, no. 4, pp. 295–306, 2010.

[6] A. Louveau, I. Smirnov, T. J. Keyes, et al., "Structural and functional features of central nervous system lymphatic vessels," *Nature*, vol. 523, pp. 337–341, 2015.

[7] J. Rustenhoven and J. Kipnis, "Bypassing the blood–brain barrier," *Science*, vol. 366, no. 6472, pp. 1448–1449, 2019.

[8] R. Rua and D. B. McGavern, "Advances in meningeal immunity," *Trends Mol. Med.*, vol. 24, no. 6, pp. 542–559, 2018.
[9] O. Semyachkina-glushkovskaya, A. Abdurashitov, A. Dubrovsky, et al., "Photobiomodulation of lymphatic drainage and clearance: perspective strategy for augmentation of meningeal lymphatic functions," *Biomed. Opt. Express*, vol. 11, pp. 725–734, 2020.
[10] O. Semyachkina-Glushkovskaya, A. Abdurashitov, M. Klimova, et al., "Photostimulation of cerebral and peripheral lymphatic functions," *Transl. Biophotonics*, vol. 597, p. e201900036, 2020.
[11] O. Semyachkina-Glushkovskaya, S. Sokolovski, and A. Noghero, "Non-invasive photosensitiser-free laser treatment of glioblastoma in rat brain," *Nat. Commun.*, 2021 (under review).
[12] S. D. Zakharov and A. V. Ivanov, "Light-oxygen effect in cells and its potential applications in tumour therapy (review)," *Quant. Electron.*, vol. 29, no. 12, p. 1031, 1999.
[13] S. G. Sokolovski, S. A. Zolotovskaya, A. Goltsov, C. Pourreyron, A. P. South, and E. U. Rafailov, "Infrared laser pulse triggers increased singlet oxygen production in tumour cells," *Sci. Rep.*, vol. 3, no. 1, p. 3484, 2013.
[14] B. Ortega-Berlanga, C. Gonzalez, and G. Navarro-Tovar, "Recent advances in the use of lipid-based nanoparticles against glioblastoma multiforme," *Arch. Immunol. Ther. Exp. (Warsz)*, vol. 69, no. 1, pp. 1–20, 2021.
[15] L. Kong, X.-T. Li, Y.-N. Ni, et al., "Transferrin-modified osthole pegylated liposomes travel the blood–brain barrier and mitigate Alzheimer's disease-related pathology in APP/PS-1 Mice," *Int. J. Nanomed.*, vol. 15, pp. 2841–2858, 2020.
[16] J.Q. Gao, Q. Lv, L.-M. Li, et al., "Glioma targeting and blood–brain barrier penetration by dual-targeting doxorubincin liposomes," *Biomaterials*, vol. 34, no. 22, pp. 5628–5639, 2013.
[17] D. Zou, W. Wang, D. Lei, et al., "Penetration of blood-brain barrier and antitumor activity and nerve repair in glioma by doxorubicin-loaded monosialoganglioside micelles system," *Int. J Nanomed.*, vol. 12, pp. 4879–4889, 2017.
[18] D. Tretiakova, E. Svirshchevskaya, N. Onishchenko, et al., "Liposomal formulation of a melphalan lipophilic prodrug: studies of acute toxicity, tolerability, and antitumor efficacy," *Curr. Drug Deliv.*, vol. 17, pp. 312–323, 2020.
[19] S. Li, N. Xiao, X. Zhang, and L. Liu, "Effects of exogenous ganglioside-1 on learning and memory in a neonatal rat model of hypoxia-ischemia brain injury," *Neural Regen. Res.*, vol. 3, no. 9, pp. 1004–1009, 2008.
[20] R.W. Ledeen and G. Wu, "The multi-tasked life of GM1 ganglioside, a true factotum of nature," *Trends Biochem. Sci.*, vol. 40, no. 7, pp. 407–418, 2015.
[21] M. L. Allende and R. L. Proia, "Lubricating cell signaling pathways with gangliosides," *Curr. Opin. Struct. Biol.*, vol. 12, no. 5, pp. 587–592, 2002.
[22] C. Zhang, W. Feng, E. Vodovozova, et al., "Photodynamic opening of the blood-brain barrier to high weight molecules and liposomes through an optical clearing skull window," *Biomed. Opt. Express*, vol. 9, no. 10, pp. 4850–4862, 2018.
[23] S. Da Mesquita, A. Louveau, A. Vaccari, et al., "Functional aspects of meningeal lymphatics in ageing and Alzheimer's disease," *Nature*, vol. 560, pp. 185–191, 2018.
[24] A. Aspelund, S. Antila, S. T. Proulx, et al., "A dural lymphatic vascular system that drains brain interstitial fluid and macromolecules," *J. Exp. Med.*, vol. 212, no. 7, pp. 991–999, 2015.
[25] H. Widner, G. Moller, and B. B. Johansson, "Immune response in deep cervical lymph nodes and spleen in the mouse after antigen deposition in different intracerebral sites," *Scand. J. Immunol.*, vol. 28, no. 5, pp. 563–571, 1988.
[26] C. Harling-Berg, P. M. Knopf, J. Merriam, and H. F. Czerr, "Role of cervical lymph nodes in the systemic humoral immune response to human serum albumin microinfused into rat cerebrospinal fluid," *J. Neuroimmunol.*, vol. 25, no. 2, pp. 185–193, 1989.
[27] P. Zhao, Z. Le, L. Liu, and Y. Chen, "Therapeutic delivery to the brain via the lymphatic vasculature," *Nano Lett.*, vol. 20, no. 7, pp. 5415–5420, 2020.
[28] N. J. Abbott, "Evidence for bulk flow of brain interstitial fluid: significance for physiology and pathology," *Neurochem. Int.*, vol. 45, pp. 545–552, 2004.
[29] J. J. Iliff and M. Nedergaard, "Is there a cerebral lymphatic system?" *Stroke*, vol. 44, no. 6, pp. 93–95, 2013.
[30] A. Louveau, B. A. Plog, S. Antila, K. Alitalo, M. Nedergaard, and J. Kipnis, "Understanding the functions and relationships of the glymphatic system and meningeal lymphatics," *J. Clin. Invest.*, vol. 127, no. 9, pp. 3210–3219, 2017.
[31] O. Semyachkina-Glushkovskaya, I. Fedosov, and A. Shirokov, "Pilot identification of the initial lymphatic capillaries in the affected human brain," *Sci. Adv.*, 2021 (under review).
[32] O. Semyachkina-Glushkovskaya, V. Chehonin, E. Borisova, et al., "Photodynamic opening of the blood-brain barrier and pathways of brain clearing," *J. Biophotonics*, vol. 11, no. 8, p. e201700287, 2018.
[33] D. F. Quail and J. A. Joyce, "The microenvironmental landscape of brain tumors," *Canc. Cell*, vol. 31, pp. 326–341, 2017.
[34] J. Song, S.-S. Lee, S. Lim, and S. Yeo, "Mechanism of the neuroprotective effect of injecting brain cells on st36 in an animal model of Parkinson's disease," *Neurosci. Lett.*, vol. 717, p. 134698, 2020.
[35] M. Hennessy and M. R. Hamblin, "Photobiomodulation and the brain: a new paradigm," *J. Opt.*, vol. 19, no. 1, p. 013003, 2017.
[36] C. E. Tedford, S. DeLapp, S. Jacques, and J. Anders, "Quantitative analysis of transcranial and intraparenchymal light penetration in human cadaver brain tissue," *Laser Surg. Med.*, vol. 47, no. 4, pp. 312–322, 2015.
[37] T. Wang, D. G. Ouzounov, C. Wu, et al., "Three-photon imaging of mouse brain structure and function through the intact skull," *Nat. Methods*, vol. 15, no. 10, pp. 789–792, 2018.
[38] D. Y. Li, et al., "Photostimulation of lymphatic clearance of red blood cells from the mouse brain after intraventricular hemorrhage," *Nat. Commun.*, 2021 (under review), https://doi.org/10.1101/2020.11.16.384149.
[39] T. I. Karu, L. V. Pyatibrat, and N. I. Afanasyeva, "Cellular effects of low power laser therapy can be mediated by nitric oxide," *Laser Surg. Med.*, vol. 36, no. 4, pp. 307–314, 2005.
[40] F. Murad, "Discovery of some of the biological effects of nitric oxide and its role in cell signaling," *Biosci. Rep.*, vol. 24, nos 4-5, pp. 452–474, 2004.
[41] I. Boldyrev, X. Zhai, M. M. Momsen, H. L. Brockman, R. E. Brown, and J. G. Molotkovsky, "New BODIPY lipid probes for fluorescence studies of membranes," *J. Lipid Res.*, vol. 48, no. 7, pp. 1518–1532, 2007.
[42] A. Shirokov, A. Fomin, and O. Semyachkina-Glushkovskaya, "Fluorescent glioma cell line and method for production thereof," Russian Federation. RU 2699754 C1: 9 (in Russian), 2019. Available at: https://patents.google.com/patent/RU2699754C1/ru.

[43] M. Wienisch, D. G. Blauvelt, T. F. Sato, and F. N. Murthy, "Two-photon imaging of neural activity in awake, head-restrained mice," *Neuromethods*, vol. 67, pp. 45–60, 2021.
[44] J. Schindelin, I. Arganda-Carreras, E. Frise, et al., "Fiji: an open-source platform for biological-image analysis," *Nat. Methods*, vol. 9, no. 7, pp. 676–682, 2012.
[45] A. Namykin, N. A. Shushunova, M. V. Ulanova, O. V. Semyachkina-Glushkovskaya, V. V. Tuchin, and I. V. Fedosov, "Intravital molecular tagging velocimetry of cerebral blood flow using Evans Blue," *J. Biophotonics*, vol. 11, no. 8, p. e201700343, 2018.
[46] H. Wang and T. Lai, "Optimization of Evans Blue quantitation in limited rat tissue samples," *Sci. Rep.*, vol. 4, p. 6588, 2014.